



## OPEN ACCESS

## EDITED BY

Yifan Li,  
China University of Geosciences, China

## REVIEWED BY

Jiawang Ge,  
Southwest Petroleum University, China  
Sarp Karakaya,  
Chevron, United States  
Shuyuan Shi,  
Research Institute of Petroleum Exploration  
and Development (RIPED), China

## \*CORRESPONDENCE

Feng Wenjie,  
✉ fwj1017@yangtzeu.edu.cn

RECEIVED 23 May 2024

ACCEPTED 25 September 2024

PUBLISHED 14 October 2024

## CITATION

Wenjie F and Ye Z (2024) Sedimentary characteristics and reservoir architecture of a lacustrine mixed carbonate/siliciclastic system: the lower member of the ShangGanchaigou Formation, Neogene, in the western Qaidam Basin, China. *Front. Earth Sci.* 12:1437205. doi: 10.3389/feart.2024.1437205

## COPYRIGHT

© 2024 Wenjie and Ye. This is an open-access article distributed under the terms of the [Creative Commons Attribution License \(CC BY\)](https://creativecommons.org/licenses/by/4.0/). The use, distribution or reproduction in other forums is permitted, provided the original author(s) and the copyright owner(s) are credited and that the original publication in this journal is cited, in accordance with accepted academic practice. No use, distribution or reproduction is permitted which does not comply with these terms.

# Sedimentary characteristics and reservoir architecture of a lacustrine mixed carbonate/siliciclastic system: the lower member of the ShangGanchaigou Formation, Neogene, in the western Qaidam Basin, China

Feng Wenjie\* and Zhang Ye

School of Geosciences, Yangtze University, Wuhan, China

Lacustrine mixed carbonate/siliciclastic sediment is an important type of oil and gas reservoir with significant potential. Although previous studies have investigated the sedimentary characteristics of the mixed depositional system in numerous oil and gas-bearing basins worldwide, a detailed sedimentary architecture model is still lacking for guiding reservoir characterization at the hydrocarbon reservoir scale. In this paper, a typical lacustrine mixed carbonate/siliciclastic sedimentary system, preserved in the lower member of the ShangGanchaigou Formation, Neogene, in the western Qaidam Basin, Western China, was deeply investigated based on well logging data from 640 wells, 438 m of cores from 3 core wells, and outcrop studies. The results demonstrate that 1) seven types of architecture elements, namely, distributary channel, channel mouth bar, distal bar, sheet-like sand, shallow water mud, algal mound, and marl flat characterized by different lithofacies associations, were recognized based on core and well logging data. 2) The lacustrine mixed carbonate/siliciclastic depositional system can be divided into three facies belts. Along the lakeward direction, the proximal facies belt is dominated by delta front deposits and characterized by gradually downstream bifurcating distributary channels and associated lateral amalgamated delta lobes. The middle facies belt is characterized by isolated and small-scale delta lobes and inter-lobe deposits, including sheet-like sand, small-scale algal mounds, and marl flats, and the distal facies belt is a combination of large-scale algal mounds and marl flats. 3) Within a depression, short-term base-level cycles controlled the facies belt transition, and the proximal, middle, and distal facies belts formed under relatively low, middle, and high base-level conditions, respectively. 4) The scale and connectivity of reservoirs gradually decreased from the proximal to the distal belt.

## KEYWORDS

mixed siliciclastic, carbonate sediments, sedimentary architecture, sedimentary model, Qaidam Basin, base-level cycle

## 1 Introduction

The mixed carbonate/siliciclastic depositional systems are widely distributed in marine and terrestrial environments (Dolan, 1989; Xu et al., 2019; Li Y et al., 2021; Karakaya et al., 2022; Lebrec et al., 2023). There are four types of mixing of clastic and carbonate sediments: punctuated mixing, facies mixing, *in situ* mixing, and source mixing (Mount, 1984). In the mixed depositional system, gravel-to-sandy deposits and permeable carbonate deposits formed large-scale reservoirs, while muddy and impermeable carbonate deposits formed stable and effective cap rock. Therefore, the mixed depositional systems can form large-scale oil and gas traps with good potential for oil and gas resources (Dolan, 1989; Chen et al., 2015; Zhao, 2015; Wei et al., 2021; Wu et al., 2022; Cui et al., 2023; Mutti et al., 2023; Kjöll et al., 2024; Karakaya et al., 2024). In the past decades, a marine mixed carbonate/siliciclastic sedimentary system was deeply investigated based on modern and ancient sedimentary records (Mount, 1984; Mount, 1985; Dolan, 1989; Lee and Kim, 1992; Lebrec et al., 2023). However, the lacustrine mixed carbonate/siliciclastic depositional systems were poorly understood due to the development conditions and limited preserved sedimentary records (Feng et al., 2013; Li Y et al., 2021; Li Q et al., 2021; Chen et al., 2022; Wu et al., 2022).

In recent years, lacustrine mixed carbonate/siliciclastic depositional records were widely observed along the margin of terrestrial depression basins such as the Bohai Bay Basin, Junggar Basin, and Qaidam Basin in China and the Williston Basin in North America (Palermo et al., 2008; Li et al., 2009; Meng et al., 2009; Feng et al., 2013; Zhao, 2015; Gao et al., 2018). Facies mixing resulting from facies belt transitions and *in situ* mixing caused by the activity of algal biota and clastic sediment deposition are the primary mixing types in depressions (Feng et al., 2013; Gierlowski-Kordesch et al., 2014; Chen et al., 2015; Du et al., 2020). Sedimentary characteristics and the diversity of lacustrine mixed carbonate/siliciclastic depositional systems were investigated in numerous studies. Basin-scale sedimentary models were found in large-scale oil and gas-bearing basins worldwide (Feng et al., 2011a; Feng et al., 2011b; Wu et al., 2019; Ye et al., 2019; Fu et al., 2020; Wang J et al., 2020; Wang Q et al., 2020). However, the detailed sedimentary characteristics and depositional model focus on the hydrocarbon reservoir scale are poorly understood. A detailed sedimentary architecture model for subsurface reservoir characterization is urgently needed.

In this paper, we deeply investigated the sedimentary characteristics and sedimentary architecture of the lacustrine mixed carbonate/siliciclastic system preserved in the lower member of the ShangGanchaigou Formation, Neogene, in the western Qaidam Basin. Lithofacies were identified from core data, and lithofacies associations were further recognized for classifying sedimentary architecture elements. A 3D outcrop model and an orthophoto projection image were produced utilizing a drone. Spatial patterns and the evolution of the lacustrine mixed carbonate/siliciclastic system in the target interval were detailed. A detailed and reliable sedimentary architecture model of a lacustrine mixed carbonate/siliciclastic system was established

based on the comprehensive analysis of subsurface reservoir data and outcrop data.

## 2 Geological settings

The Qaidam Basin is a large-scale oil and gas-bearing basin located north of the Qinghai-Tibet Plateau, Western China (Figure 1). It is a Mesozoic and Cenozoic continental basin (Feng et al., 2013). The study area includes a subsurface oil and gas reservoir and an outcrop. The subsurface reservoir within the Huatugou Oilfield and the outcrop in the Ganchaigou area are distributed in the western part of the Qaidam Basin. The target interval of the study is the facies mixing types of mixed deposits and the VI and VII oil zones of the lower member of the ShangGanchaigou Formation, Neogene (Figure 2). There is slight compositional mixing, but it is atypical. During the early Neogene, the Qaidam Basin was a depression characterized by shallow lacustrine deposition (Zhang et al., 2004; Wu et al., 2019). The western Altun Mountains and the western Qimantag Mountain supplied adequate clastic sediments, and the sediments were transported from the end of the west of the basin to the depression (Figure 1).

During the sedimentation of the target interval, the paleoclimate is arid (Zhang et al., 2004; Chen et al., 2004; Li et al., 2009; Wang et al., 2012). The fossil assemblage identified from the cores is Eucypris-Youshashania-Hemicyprirotus, indicating shallow and semi-saline-saline water at the margin of the depression (Li et al., 2020). During the deposition of the target interval, the average paleo-salinity was 1.27%, and the maximum paleo-salinity was 2.66% (Chen et al., 2015). The arid paleo-climate, high salinity, and shallow water provided favorable carbonate production conditions (Chen et al., 2015; Chen et al., 2022; Li et al., 2020). The target interval is approximately 150 m thick and can be divided into 41 single-layer units. Three middle-term base-level cycles (MSC1-MSC3) and nine short-term base-level cycles (SSC1-SSC9) were recognized based on well logging and core data (Figure 2). According to previous research, the study area is located at the transformation zone between the upstream deltas and lakeward algal mound (AM)-marl flats (MFs) (Zhang et al., 2004).

## 3 Results

### 3.1 Lithofacies, lithofacies associations, and interpretations

#### 3.1.1 Core lithofacies

Based on lithological characteristics, sediment structures, and rock colors, seven lithofacies were observed from 438 m of the core of three core wells, as shown in Figure 1C. Typical core images and thin-section images are shown in Figure 3.

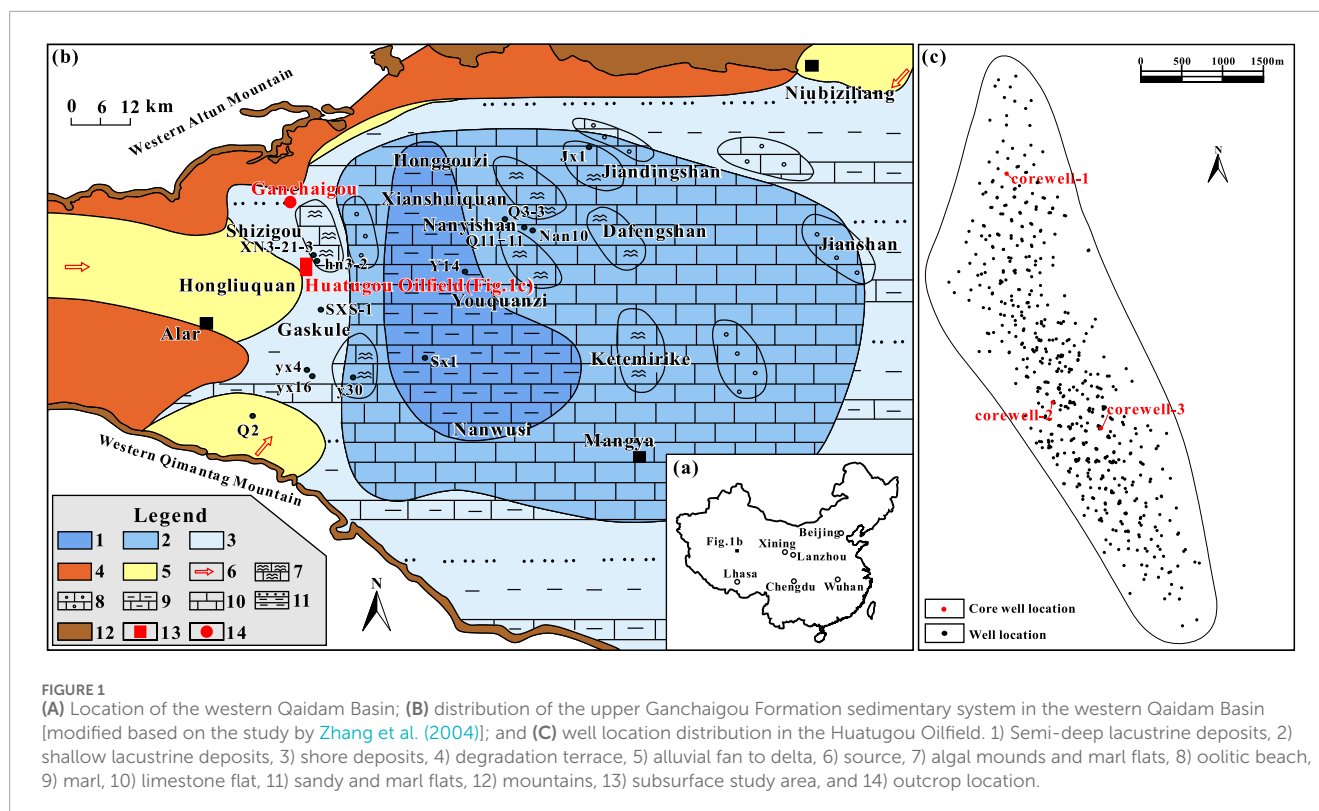


FIGURE 1

(A) Location of the western Qaidam Basin; (B) distribution of the upper Ganchaigou Formation sedimentary system in the western Qaidam Basin [modified based on the study by Zhang et al. (2004)]; and (C) well location distribution in the Huatugou Oilfield. 1) Semi-deep lacustrine deposits, 2) shallow lacustrine deposits, 3) shore deposits, 4) degradation terrace, 5) alluvial fan to delta, 6) source, 7) algal mounds and marl flats, 8) oolitic beach, 9) marl, 10) limestone flat, 11) sandy and marl flats, 12) mountains, 13) subsurface study area, and 14) outcrop location.

### 3.1.1.1 Facies 1—massive bedding gravel—coarse sandstone

Facies 1 (F1) is characterized by poorly sorted gravel clastic, fine-coarse sand, and muddy sediments. The proportion of gravel debris is 5%–30%, with particle diameters ranging from 2 mm to 25 mm, usually consisting of brown or gray metamorphic debris (Figure 3A). Mud pebble was observed in a low ratio of F1 (Figure 3B), which reveals the existence of reworking and short-distance redeposition of pre-existing muddy sediment. Predominant sedimentary structures of F1 are massive bedding, with occasional occurrences of trough cross-bedding. F1 is formed under the action of strong tractional flows, and its thickness is approximately 0.5–5.0 m. The commonly observed upward-fining trend indicates that F1 belongs to channel deposits. In order to track and measure the scale of the lithofacies unit, well correlation sections with a well spacing of 20–100 m are built and analyzed. The lateral tracking of the F1 unit in the subsurface reservoir shows a width of approximately 100–200 m.

### 3.1.1.2 Facies 2—massive bedding medium sandstone

Facies 2 (F2) is characterized by well-sorted medium sand. Muddy sediment content is relatively low (Figure 3C). The main sedimentary structure is massive bedding. Due to low compaction and cementation, the details of sedimentary structures are difficult to observe. The thickness of an F2 unit is approximately 0.2–1.0 m. Usually, several F2 units are vertically stacked to form large-scale sand layers with a thickness of 2.0–8.0 m. According to core observation and well logging data analysis, F2 is generally distributed within channel or channel mouth bar (CMB) deposits. Occasionally, there are mud interlayers

between two F2 units. The lateral tracking results of subsurface reservoirs show that the width of F2 units can reach several hundred meters.

### 3.1.1.3 Facies 3—massive bedding fine sandstone

Facies 3 (F3) is characterized by well-sorted, fine sand (Figure 3D). Muddy sediment content is slightly higher than that in F2. Massive bedding is recognized from cores, indicating that F3 is formed in relatively open waters near the channel mouth and unaffected by waves. The thickness of an F3 unit is generally below 0.5 m, and the unit is separated by consistently distributed mudstone in the vertical direction. In subsurface reservoirs, F3 units are mainly distributed along the edge of F2.

### 3.1.1.4 Facies 4—interbedded siltstone—mudstone with deformed bedding, wavy bedding, and a bioturbation structure

Facies 4 (F4) is characterized by interbedded siltstone and mudstone (Figures 3E, F). The thickness of a siltstone or mudstone layer is approximately 0.5–5 cm. Alternating changes in siltstone and mudstone indicate the frequent hydrodynamic variations in the area far from the channel mouth. Wavy bedding is formed by the force of waves in open waters (Figure 3E). Suspended sediments, including mud and silt, are alternately deposited with the change in upstream channel systems and lake currents. Due to the shallow water depth, burrow pores with varied directions reworked the siltstone and mudstone (Figure 3F). Mudstone in F4 is usually red, demonstrating that the water depth is very shallow and the water level fluctuates frequently.

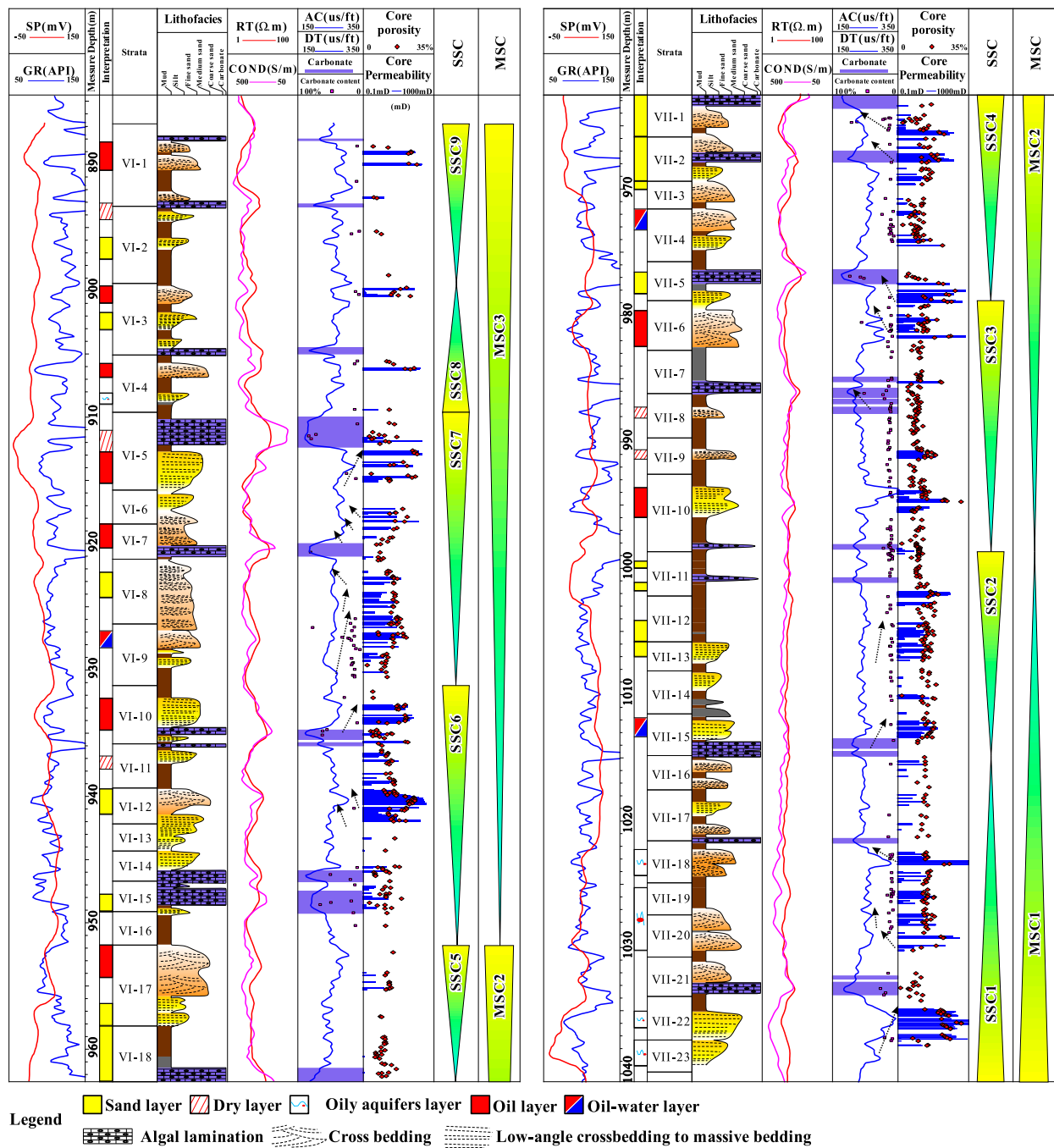


FIGURE 2 Stratigraphic column for VI–VII oil groups in the ShangGanchaigou Formation, Huatugou Oilfield. The interpretations of sedimentary characteristics and base-level cycles are based on continuous core data and well logging data. The core well is corewell-2, as shown in Figure 1C.

### 3.1.1.5 Facies 5—mudstone with horizontal bedding and muddy pebbles

Facies 5 (F5) is characterized by dark mudstone with horizontal bedding, which is formed under static water (Figure 3G). Floating mud pebbles and fine gravel clastic are recognized in a low ratio of F5 units (Figure 3H), indicating the presence of storm events (Chen et al., 2022). Compared to F4, F5 is

formed in a deeper lake area, significantly further away from the channel mouth.

### 3.1.1.6 Facies 6—stromatolitic algal limestone

Facies 6 (F6) is characterized by stromatolitic algal limestone, and typical stromatolite pillars are observed on cores (Figures 3I, J, L). Thin-section observations suggest that



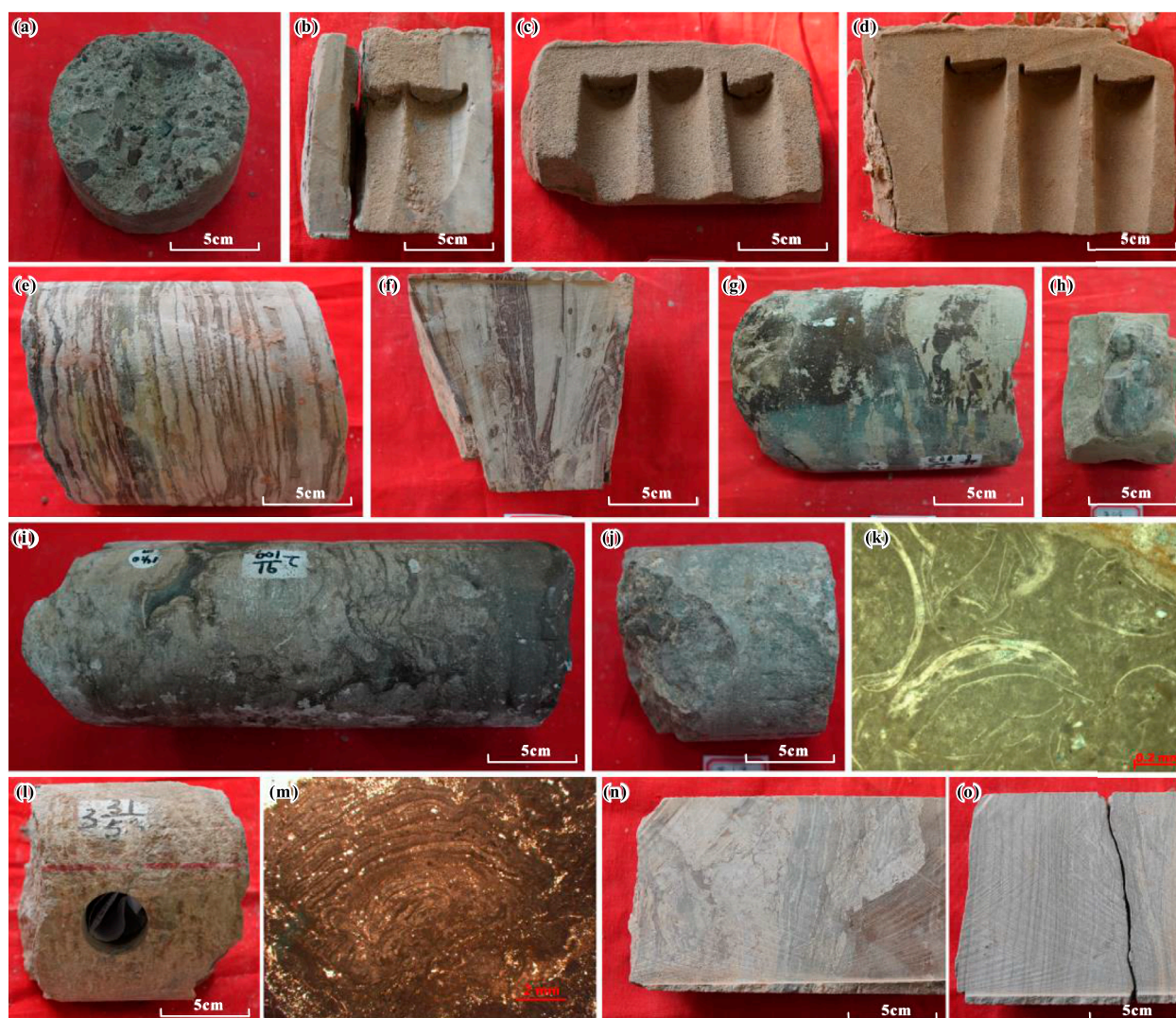


**FIGURE 3**

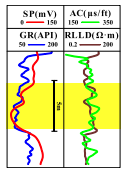
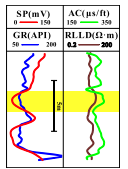
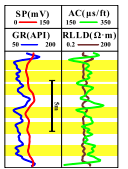
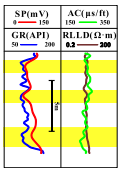
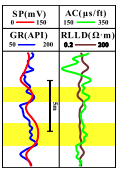
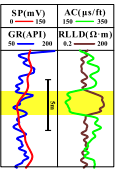
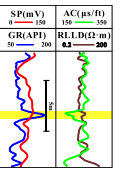
Typical core images and microscopic pictures of the mixed sedimentary record. **(A)** Core from corewell-1 with massive bedding of gravel-coarse sandstone and a core depth of 1,394.15 m. **(B)** Core from corewell-2 with massive bedding of gravel-coarse sandstone and a core depth of 968.05 m. **(C)** Core from corewell-2 with massive bedding of medium sandstone and a core depth of 1,033.21 m. **(D)** Core from corewell-2 with massive bedding of fine sandstone and a core depth of 931.53 m. **(E)** Core from corewell-3 with interbedded siltstone-mudstone with deformed bedding, wavy bedding, and a bioturbation structure and a core depth of 986.39 m. **(F)** Core from corewell-3 with interbedded siltstone-mudstone with deformed bedding, wavy bedding, and a bioturbation structure and a core depth of 1,009.25 m. **(G)** Core from corewell-2 with mudstone with horizontal bedding and muddy pebbles and a core depth of 1,417.11 m. **(H)** Core from corewell-2 with mudstone with horizontal bedding and muddy pebbles and a core depth of 1,418.72 m. **(I)** Core from corewell-1 with stromatolitic algal limestone and a core depth of 1,389.72 m. **(J)** Core from corewell-1 with stromatolitic algal limestone and a core depth of 1,375.39 m. **(K)** Core from corewell-1 with stromatolitic algal limestone and a core depth of 1,375.43 m. **(L)** Core from corewell-3 with stromatolitic algal limestone and a core depth of 961.45 m. **(M)** Core from corewell-1 with stromatolitic algal limestone and a core depth of 1,537.83 m. **(N)** Core from corewell-2 with marl with horizontal bedding and deformed bedding and a core depth of 902.35 m. **(O)** Core from corewell-2 with marl with horizontal bedding and deformed bedding and a core depth of 903.42 m. Locations of the three core wells are given in [Figure 1C](#).

bioclasts, mud, and carbonate sediment filled the spaces between stromatolite pillars ([Figure 3K](#)). In some thin sections, growth laminae within the stromatolites are also discernible ([Figure 3M](#)). The thickness of an F6 unit ranges from 0.5 to 5.0 m, and the width of F6 can reach hundreds of meters in subsurface reservoirs. In some instances, carbonate sediments within F6 units have undergone dissolution, leading to the formation of larger-scale pores, thereby becoming high-quality reservoirs.

### 3.1.1.7 Facies 7—marl with horizontal bedding and deformed bedding

Facies 7 (F7) is characterized by horizontal-bedding marl and deformed bedding ([Figure 3N, O](#)). During marl formation, hydrodynamic forces were weak, and the water depth was significantly deeper than that of F6, resulting predominantly in horizontal bedding. Most marls are subject to varying degrees of deformation due to compaction effects and/or storm-related activity, giving rise to the coexistence of deformed and horizontal bedding.

**TABLE 1** Typical well logging patterns, lithologies, sedimentary structures, and sedimentary rhythm of the facies belts and microfacies in the mixed sedimentary system. The yellow intervals are the recognized elements.

Facies belt	Delta front					Prodelta	
Architecture element	Distributary channel	Channel mouth bar	Distal bar	Sheet-like sand	Shallow-water mud	Algal mound	Marl flat
Typical well logging pattern							
Lithology	Gravel, pebbled sandstone, and coarse-medium sandstone	Coarse-fine sandstone	Fine sandstone and muddy siltstone	Muddy siltstone	Mudstone	Algal limestone	Marl
Lithofacies associations	F1 + F2	F2 + F3 + F4	F3 + F4	F4	F5	F6	F7
Sedimentary structure	Massive bedding, parallel bedding, and scour and filling	Massive bedding and low-angle cross-bedding	Massive bedding, wavy bedding, and bioturbation structure	Wavy bedding, horizontal bedding, and bioturbation structure	Massive bedding, horizontal bedding, and bioturbation structure	Algal-laminated	Horizontal bedding and deformation
Sedimentary rhythm	Positive, homogeneous	Negative	Negative	Negative, homogeneous	Homogeneous	-	-
Thickness (m)	2.0–5.0	2.0–5.0	0.5–2.0	0.2–0.5	-	0.5–5.0	0.2–0.5

### 3.1.2 Lithofacies associations and architecture elements

To characterize the sedimentary architecture of the target interval, the lithofacies associations and corresponding architecture elements were recognized based on well logging patterns, lithofacies associations, and sedimentary rhythms (Table 1). The well logging patterns consist of spontaneous potential (SP), gamma ray (GR), acoustic (AC), deep induction resistivity (RILD) curves, and yellow interpreted elements. The patterns were built based on core description and core-well logging correlation analysis. The sedimentary characterization observed in core and subsurface reservoir data shows that the lacustrine mixed carbonate/siliciclastic system was composed by clastic sediments of the braided river delta and carbonate sediments of the algal mound and marl flat deposits. Seven architecture elements distributed from the delta front to the prodelta were recognized.

#### 3.1.2.1 Distributary channel

Distributary channels (DCs) distribute from the delta plain to the delta front, transporting clastic sediments to the downstream areas. Due to the strong hydrodynamic force of channelized flow, the coarsest sediments (F1) are deposited at the bottom of active channels. As the river continues to evolve, its water flow tends to decrease, leading to a gradual decrease in the sediment particle size and the formation of relatively fine sediment (F2). Therefore, the DC units observed from well logs are characterized by a positive to homogeneous rhythm (Table 1). From the bottom to the top, the lithofacies type transforms from F1 to F2, and the gradually

increasing GR presents the upward fining trend of the particle size. Due to the downstream bifurcation of the channel system, the scale of channels decreased along the flow direction.

#### 3.1.2.2 Channel mouth bar

The channel mouth bar is formed by the continuous feeding of distributary channels and the deposition of upward coarsening sediments with their progradation. In subsurface reservoirs, CMBs are distributed along or ahead of DCs to form DC-CMB lobes. F4, F3, and F2 form a typical CMB from the bottom to the top, respectively (Table 1). Therefore, a CMB can be recognized by upward decreasing GR and the negative rhythm of the particle size from well logs. Controlled by the complex variations in DCs, the vertical lithofacies association may be repeating, inter-overlapping to form a thick CMB unit.

#### 3.1.2.3 Distal bar

A distal bar (DB) is formed along the outer edge of CMBs. Due to its deposition area being remote from channel mouths, the hydrodynamic force is relatively weak, resulting in sediments primarily comprising fine-grained suspended matter, such as fine sand, silt, and clay. A DB is composed of F4 units at the bottom and F3 units at the top (Table 1). Several muddy interlayers appear between the lithofacies units in the vertical direction. A DB exhibits a distinct negative rhythm characterized by gradually decreasing GR values from bottom to top. Still, it further reveals multiple thin, negative-rhythm layers separated by muddy interlayers (Table 1).

### 3.1.2.4 Sheet-like sand

Sheet-like sand (SS) is formed in the open waters far from channel mouths, primarily composed of suspended sediments such as silt and clay, and characterized by relatively thin thickness. Sheet-like sand deposits are typically prone to reshaping by lake waves during deposition and subsequent periods, forming randomly dispersed, isolated, thin laminae of sand bodies. The predominant lithofacies type in such deposits is F4 (Table 1). Similar to DBs, sheet-like sand units are often separated by intervals of mudstone, which effectively isolate F4 units in the vertical direction. A slight negative rhythm indicated by gradually decreasing GR values from bottom to top is the typical identification mark (Table 1).

### 3.1.2.5 Shallow water mud

Shallow water mud (SWM) is characterized by pure mudstone formed in still waters within the distal part of the delta front. Massive or horizontal bedding mudstone is re-worked by bioturbation (Table 1). A high GR value indicates a higher mud content than that of the other architectural elements.

### 3.1.2.6 Algal mound

Algal mounds formed in the clean and shallow water area in the prodelta are characterized by mound-shaped, thick-bedded algal limestone. The main lithofacies is F6. The formation of algal mounds primarily results from the accumulation of carbonate sediments produced by algal growth, mixed with bioclasts and clay, typically forming isolated, mound-shaped structures offshore. Their characteristic log response patterns include acoustic impedance (AC) values significantly lower than those of both shales and sandstones, GR readings similar to those of mudstones, and a slight negative anomaly observable in the SP (Table 1).

### 3.1.2.7 Marl flat

In contrast to algal mounds, a marl flat (MF) develops in settings with higher carbonate productivity and is primarily composed of layers of mud, along with carbonate (including limy and dolomitic) deposits, stacked in thin interbeds (Table 1). The main lithofacies type of MF is F7. They are predominantly found along the margins of algal mounds and in the distal parts of the prodelta. The MF units are significantly thinner and wider than the AM units. Owing to their high content of both clay and carbonate, their logging responses are characterized by GR values significantly higher than those of shales, AC values notably lower than those of shales, and SP readings close to the baseline (Table 1).

## 3.2 Sedimentary characteristics of the Ganchaigou outcrop

In order to investigate the spatial patterns of the mixed carbonate/siliciclastic system, a virtual 3D outcrop model was built, and a high-resolution orthographic image that vertically sliced the exposed stratum of the Ganchaigou outcrop was further created (Figure 4A). As illustrated in Figure 4A, we perform an orthographic projection on highly inclined outcrops to obtain images that reveal the true characteristics of geological stratification sections. The stratigraphic interface and boundary of algal and muddy limestone were recognized and traced on the outcrop image (Figure 4A).

The results show that the thickness of each stratum unit is constant in at least a 1,500-m-wide section. Thin algal limestone and marl layers exist within stratum units and form an interlayered pattern with the clastic rock (Figure 4A). Typical sedimentary characteristics of the outcrop are given in Figures 4B–E. Marl layers typically occur as nearly evenly thick–thin beds interbedded within clastic rock layers, with thicknesses of 0.2–0.5 m and widths extending from hundreds of meters to several kilometers (Figure 4C). Algal limestone exhibits prominent mound-like structures, typically with a flat base and a domed top, varying in thickness from 0.5 to 5.0 m, while the width of algal mound units spans from tens to hundreds of meters (Figures 4C–D). Clastic rock layers belong to deltaic deposits and typically progress upward from mudstones, through silty mudstones, to fine–coarse-grained sandstones (Figure 4F).

According to the observation of the outcrop, deltaic deposits are the predominant component of the target interval, accounting for over 80%, while algal mound and marl flat contents are relatively minor, generally occurring between accretions at the lower to middle part of channel mouth bar deposits (Figure 4B). Carbonate deposits mostly coexist with the mudstone deposited far away from deltas. The frequent transformation from clastic to carbonate deposits demonstrated that the sedimentary environment changed rapidly under arid climate conditions.

## 3.3 Spatial patterns of the mixed carbonate/siliciclastic depositional system

The architecture elements were distinguished from well logging data based on the identification of lithofacies associations. The spatial patterns of the mixed carbonate/siliciclastic depositional system were discovered, and three representative facies belts were characterized (Figure 5).

### 3.3.1 Proximal facies belt

The proximal facies belt is characterized by a multi-level branching distributary channel network and the associated channel mouth bars and distal bars (Figure 5A). A typical facies map presented in Figure 5A showed that three deltas coexist, and the average width of a delta ranges from hundreds of meters to several kilometers (Figure 5A). The widely developed distributary channel, channel mouth bar, and distal bar units within the proximal part of the delta front amalgamated laterally, forming extensive interconnected reservoirs (Figures 5A, 6). The proximal facies belt is dominated by deltas, and carbonate deposition is found only in restricted shallow-water areas between distributary channels, primarily as thin layers of marl, which are of limited extent (Figure 5A).

### 3.3.2 Middle facies belt

The middle facies belt is characterized by smaller deltas and larger-scale carbonate deposits than that of the proximal facies belt (Figure 5B). Deltas are isolated, and distributary channels exhibit a higher curvature with fewer bifurcations in general. The thickness and width of delta deposits are significantly smaller than that of the proximal facies belt (Figure 6). Marl layers exist between deltas and coexist with shallow-water mudstone. In this belt, algal



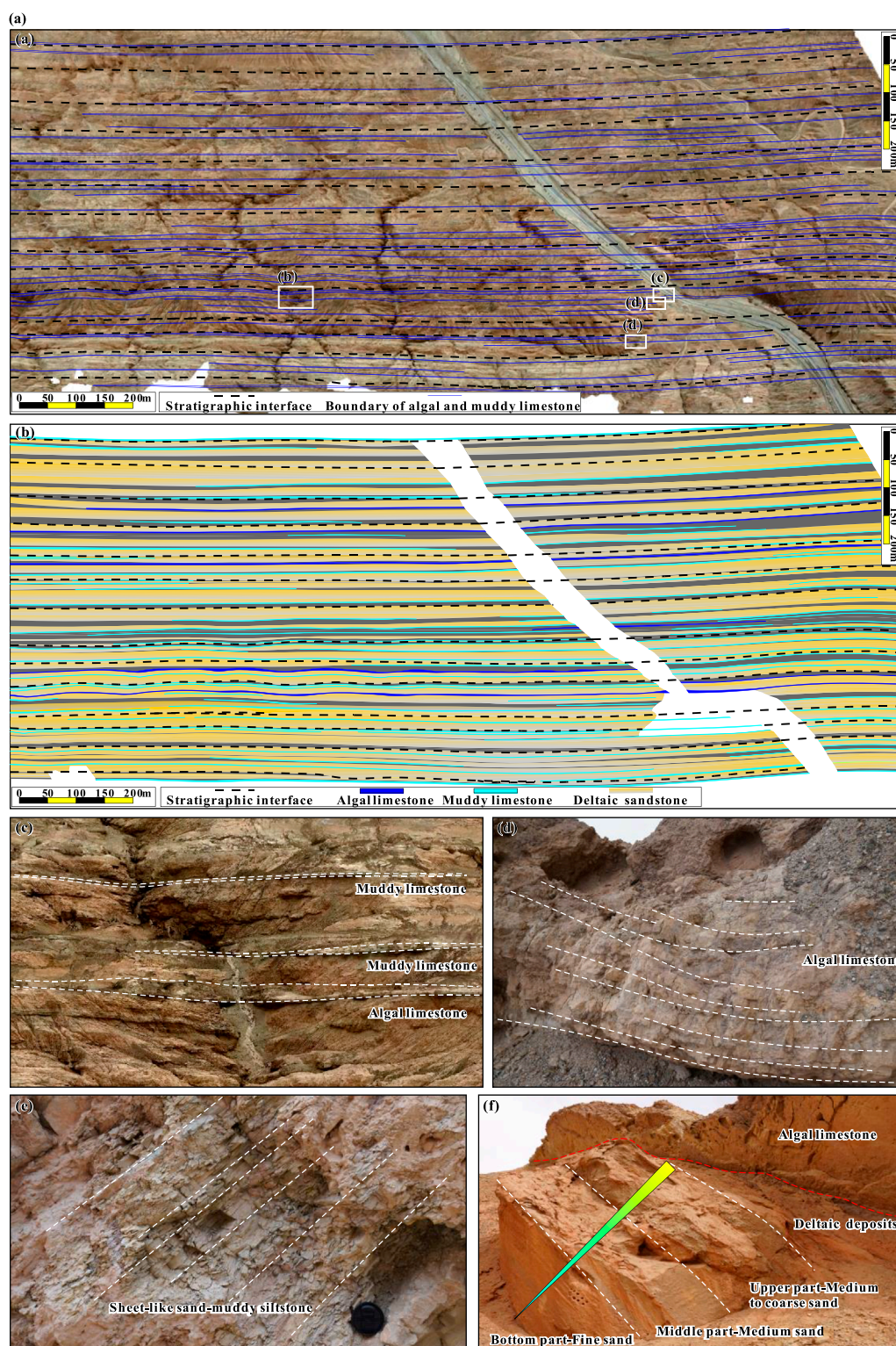


**FIGURE 4** Orthorectified aerial image and sedimentary facies analysis of the Upper Ganचाigou Formation in the Ganचाigou outcrop area. **(A)** Orthorectified aerial image. **(B)** Facies interpretation of the outcrop **(C–F)**. Typical deposits of the outcrop.

mound elements are distributed very sparingly in the broader areas between deltas, and sheet-like sand occasionally develops in the lakeward area (Figure 5B).

### 3.3.3 Distal facies belt

The distal facies belt is characterized by very limited delta deposits and large-scale algal mounds, marl flats, and sheet-like sand

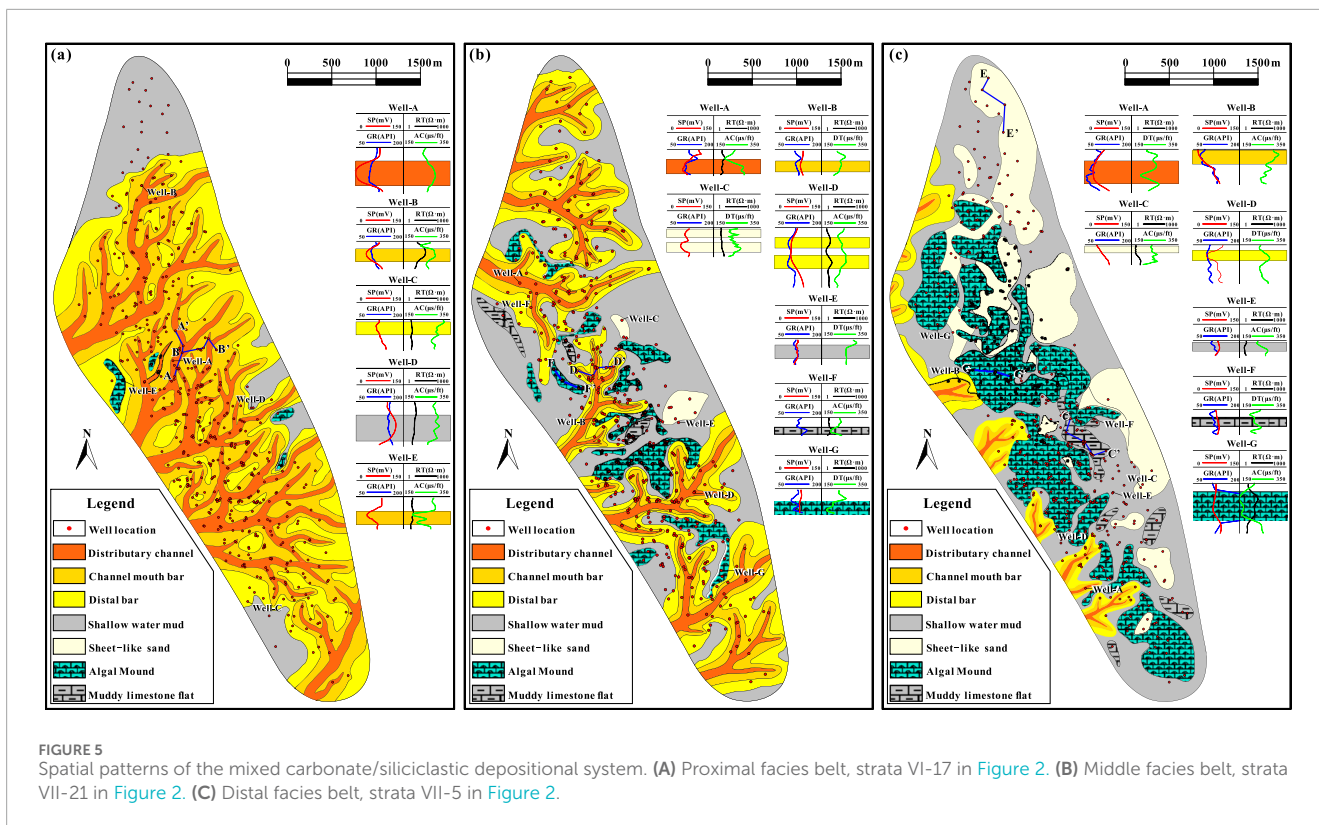


FIGURE 5 Spatial patterns of the mixed carbonate/siliciclastic depositional system. (A) Proximal facies belt, strata VI-17 in Figure 2. (B) Middle facies belt, strata VII-21 in Figure 2. (C) Distal facies belt, strata VII-5 in Figure 2.

layers (Figure 5B). This belt is located within the open waters in the prodelta, with sheet-like sand generally distributed in the lower part of the stratum unit with mudstone. Meanwhile, algal mound units are mainly distributed at the lower to middle part of the stratum unit (Figure 6). A marl flat usually develops around or between two algal mounds. The facies map and sections show that the distal facies belt is stacked by interlayered sheet-like sand, algal mounds, and marl flat units (Figures 5, 6).

## 4 Discussion

### 4.1 Sedimentary model of a lacustrine mixed carbonate/siliciclastic system

In this paper, a lacustrine mixed carbonate/siliciclastic system was discovered based on data from subsurface reservoirs and outcrops. Core lithology revealed that the mixing type of the target interval is mainly facies mixing. Compared to the marine mixed carbonate/siliciclastic system (Mutti et al., 2023; Kjøl et al., 2024), the production of carbonate deposits at the margin of the depression is limited due to the unstable salinity and clastic sediment transportation driven by changing climate. Therefore, only limited *in situ* mixing occurred (Wu et al., 2019; Wu et al., 2022; Chen et al., 2022). In the past 20 years, extensive research has discovered the sedimentary model of the lacustrine mixed carbonate/siliciclastic depositional system along the margin of depressions (Chen et al., 2004; Zhang et al., 2004; Dong et al., 2007; Li et al., 2009; Meng et al., 2009; Feng et al., 2011a; Feng et al., 2011b; Wang et al.,

2012; Wang J et al., 2020; Wei et al., 2021; Liu et al., 2021; Wu et al., 2022; Cui et al., 2023). However, the detailed sedimentary architecture and sedimentary model of the mixed deposits for subsurface reservoir characterization still need to be explored.

Within the lacustrine mixed sedimentary system, three sedimentary facies belts with significant spatial pattern variations are recognized (Figure 5). Along the lakeward direction, the mixed sedimentary system can be divided into three facies belts, namely, the proximal facies belt, dominated by the delta front; the middle facies belt, characterized by the delta front and small-scale carbonate deposits; and the distal facies belt consisting of algal mounds and marl flats (Figure 7).

Large-scale delta-front deposits characterize the proximal facies belt. Distributary channels gradually bifurcate along the lakeward direction, creating an intricate channel network. Channel mouth bars developed with the lakeward extension of bifurcating channels, forming delta lobes composed of distributary channel-channel mouth bar-distal bars, and these lobes amalgamated to form a large-scale, widely distributed, and interconnected clastic rock reservoir. Due to the arid climate, the activity of deltas is driven by flood events. As a result, carbonate deposits occasionally developed within the restricted waters between the lateral combinations during inter-flood periods (Figure 7).

The middle facies belt covered the transitional area between the delta front and prodelta. Only a few distributary channels extended into the area and formed small-scale and isolated delta lobes. Sheet-like sand, algal mounds, and marl flats developed within the area between two delta lobes. In this belt, carbonate deposits also formed during the inter-flood periods. In general,



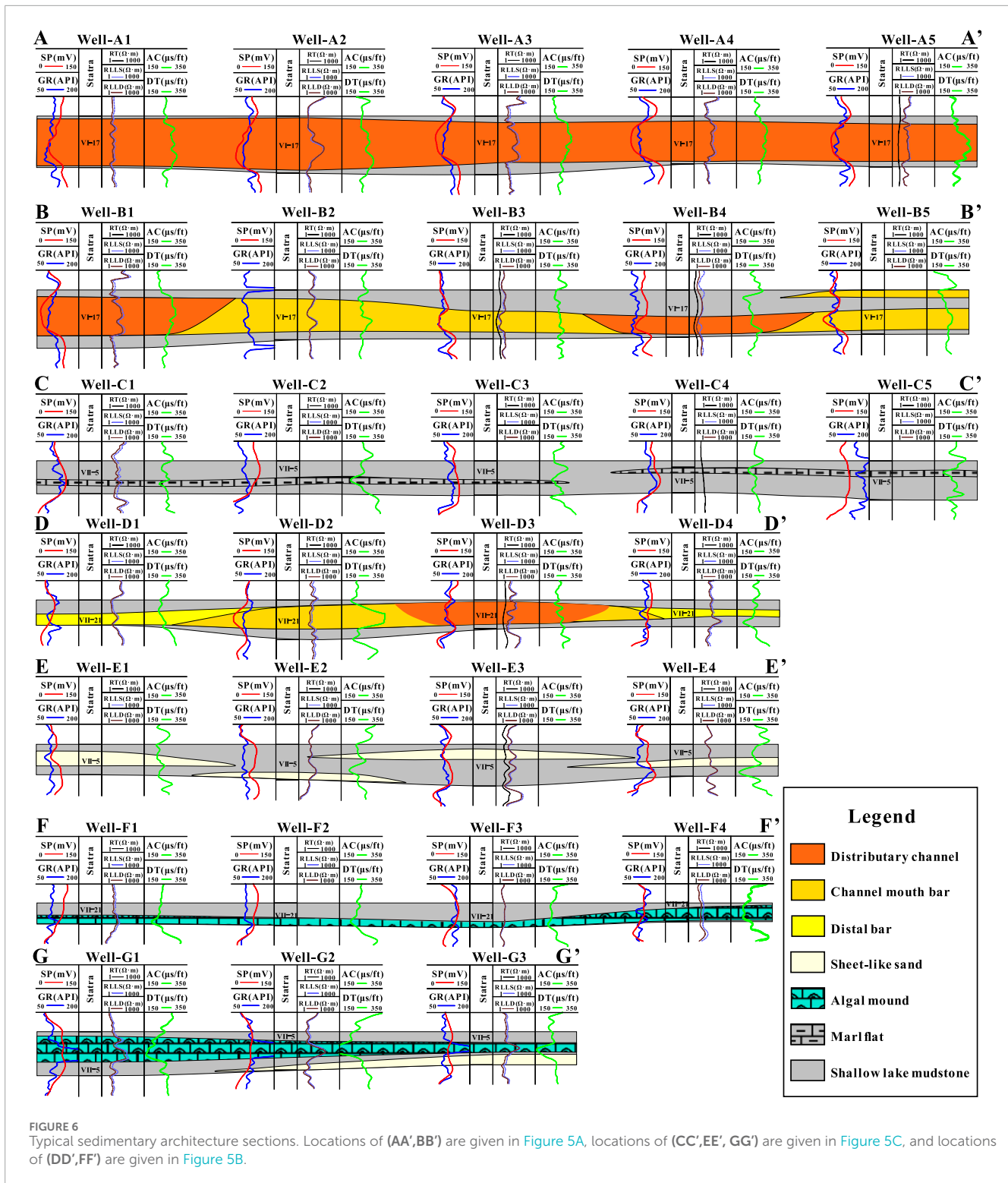
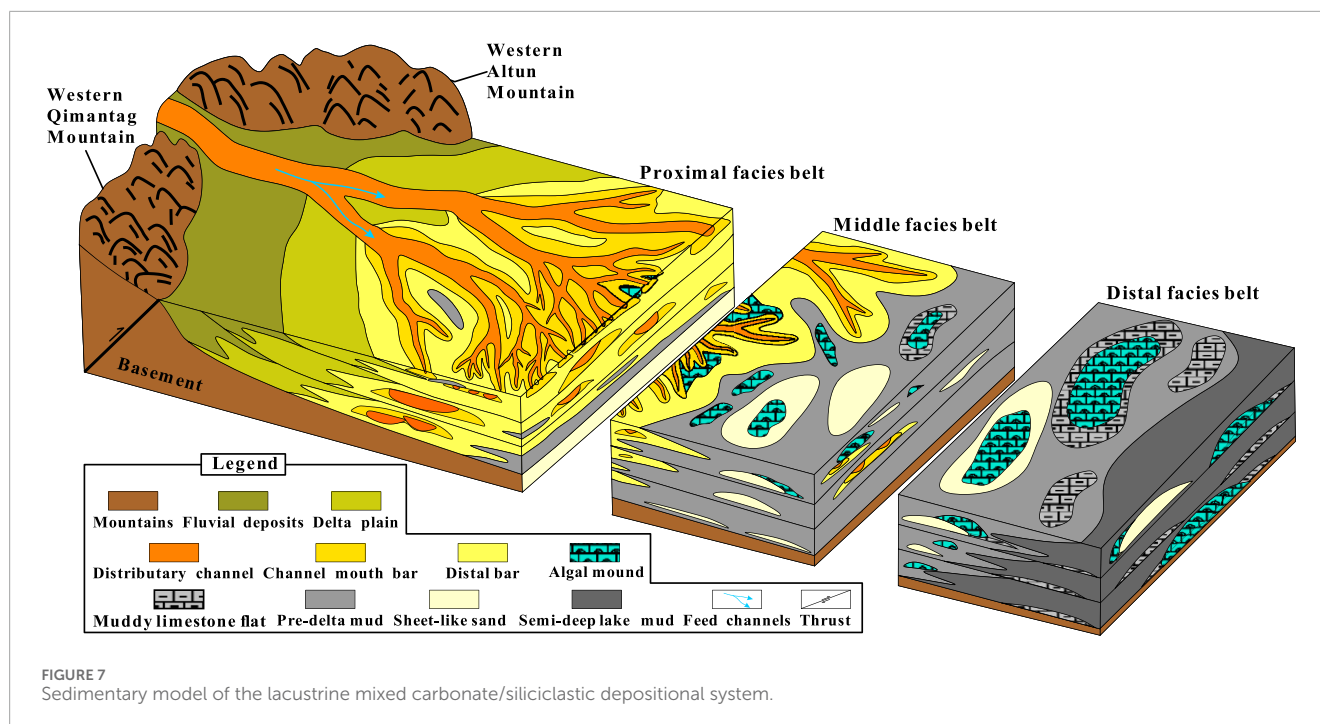


FIGURE 6 Typical sedimentary architecture sections. Locations of (AA',BB') are given in Figure 5A, locations of (CC',EE', GG') are given in Figure 5C, and locations of (DD',FF') are given in Figure 5B.

the algal mounds developed after the abandonment of the upstream deltas.

The distal facies belt forms within prodelta areas and is characterized by large-scale algal mounds and marl flats (Figure 7). Due to the area being far away from the upstream deltas, clastic deposits are mainly

suspended, transported clay and silt. Alga-generated carbonate sediments mixed with bioclasts and clay deposits to form algal mounds and marl flats. As the algal mounds and marl flats are thin-layered, multiple layers are vertically stacked to form interlayered mudstone, sheet-like sand, algal mounds, and marl flats.



In the mixed system, the main mixing type is facies mixing. There is slight compositional mixing, but it is atypical. Therefore, the deltaic reservoir within the mixed system is highly qualified (Fang, 2010). Some of the algal mounds that have undergone large-area dissolution can be regarded as reservoirs with good potential, and undissolved algal mounds and marl flats generally have extremely low permeability and can be treated as barriers to subsurface fluid flow (Chen et al., 2004).

## 4.2 Base-level fluctuations drive facies belt transition.

The base-level cycle is a comprehensive reflection of factors such as tectonic activity and climate change and a key factor driving the evolution of sedimentary systems in shallow-water areas in the lacustrine environment (Wu et al., 2019; Chen et al., 2022; Mutti et al., 2023). In a depression, due to the low intensity of tectonic activity (Wu et al., 2019; Wu et al., 2022), the paleoclimate is the dominant factor affecting the base-level cycles (Wu et al., 2019). A short-term base-level cycle is the dominant factor controlling the facies belt transformation within the study area. Three typical stratum units are taken as examples and explained below.

The distal facies belt appears at the stage of the rise-to-fall transformation of two adjacent short-term base-level cycles (Figure 2), and arid climate and relatively deep water are conducive to algae flourishing and the production of carbonate and algal mounds (Ye et al., 2019). As a result, marl flats are the dominant architectural elements in the distal facies belt (Figure 5C).

The middle facies belt is formed during the middle stage of a short-term base-level cycle (Figure 2). The water depth is generally shallower than that in the initial stage, and the production of carbonate decreases, resulting in the mixing of the terminal part of

deltas. Algal mounds and marl flats are produced on a smaller scale (Figure 5B).

The proximal facies belt is formed at the stage of the fall-to-rise transformation of two adjacent short-term base-level cycles (Figure 2). The very limited accommodation space and relatively shallow water hinder carbonate production (Ye et al., 2019) while enhancing the development of deltas (Figure 5A).

With the transformation of facies belts within a short-term-sub-short-term base-level cycle, a mixing of carbonate and siliciclastic layers in the vertical and downstream directions occurs (Figure 4).

## 5 Conclusion

This paper focuses on the discovery of the sedimentary characteristics, spatial patterns, and architecture of a lacustrine mixed carbonate/siliciclastic system at the margin of a depression based on outcrop and subsurface reservoir data.

Seven types of lithofacies, including clastic and carbonate deposits, were identified based on core data. Core data, well logging data, and outcrop data were used to establish a classification of sedimentary architecture elements distributed along the lakeward direction. Seven types of sedimentary architecture elements were identified from well data, and the spatial distribution and patterns were characterized for each single-layer unit.

The sedimentary system can be divided into three facies belts along the lakeward direction. The proximal facies belt is characterized by large-scale, widely distributed, and interconnected delta-front deposits, which are composed of lakeward bifurcating distributary channels and corresponding delta lobes. The middle facies belt is characterized by relatively small-scale isolated distributed delta lobes, sheet-like sand, and limited carbonate

deposits. The distal facies belt is dominated by algal mounds and surrounding marl flats.

Within the study area, the development of facies belts in different single-layer units is closely related to the short-term base-level cycles. The proximal and distal facies belts are formed during the fall-to-rise and rise-to-fall transformation of two adjacent short-term base-level cycles, respectively. The middle facies belt is formed during the middle stage of a short-term base-level cycle. At the margin of the depression, a short-term base-level cycle dominated the facies belt transformation during the formation of the target interval, resulting in the inter-layered vertical stacking of the three facies belts. According to the established sedimentary model, the scale, connection, and quality of reservoirs gradually decreased from the proximal to the distal facies belt.

## Data availability statement

The original contributions presented in the study are included in the article/Supplementary Material; further inquiries can be directed to the corresponding author.

## Author contributions

FW: conceptualization, data curation, formal analysis, funding acquisition, investigation, methodology, project administration, resources, software, supervision, validation, visualization,

writing—original draft, and writing—review and editing. ZY: data curation, formal analysis, funding acquisition, resources, software, validation, visualization, and writing—original draft.

## Funding

The author(s) declare that financial support was received for the research, authorship, and/or publication of this article. This research was funded by the National Natural Science Foundation of China with grant numbers 41802123 and 42130813.

## Conflict of interest

The authors declare that the research was conducted in the absence of any commercial or financial relationships that could be construed as a potential conflict of interest.

## Publisher's note

All claims expressed in this article are solely those of the authors and do not necessarily represent those of their affiliated organizations, or those of the publisher, the editors, and the reviewers. Any product that may be evaluated in this article, or claim that may be made by its manufacturer, is not guaranteed or endorsed by the publisher.

## References

- Chen, Z., Shou, J., Wang, S., and Meng, S. (2004). Tertiary lake algal limestone oil and gas reservoirs in the western part of Qaidam Basin and exploration potential. *China Pet. Explor.* 9, 59–66.
- Chen, N. G., Wang, Y. Q., Xu, F., Yang, T. Y., and Xia, Z. Y. (2015). Palaeosalinity characteristics and its sedimentary response to the Cenozoic salt-water lacustrine deposition in Qaidam Basin. *J. Palaeogeogr.* 17, 371–380. doi:10.7605/gdtxb.2015.03.31
- Chen, Y., Xia, X. M., Zhao, J., Cui, J., Qiao, B. H., Zhao, D. S., et al. (2022). Sedimentary characteristics and formation mechanisms of Neogene algal limestone in Western Qaidam Basin. *Acta Sedimentol. Sin.* 40, 1323–1334. doi:10.14027/j.issn.1000-0550.2021.056
- Cui, H., Zhu, S., Liang, C., Ma, W., Tong, H., and Shi, Z. (2023). Facies association analysis of a Toarcian siliciclastic-carbonate lacustrine system, Sichuan Basin, China. *Palaeogeogr. Palaeoclimatol. Palaeoecol.* 631, 111841. doi:10.1016/j.palaeo.2023.111841
- Dolan, J. F. (1989). Eustatic and tectonic controls on deposition of hybrid siliciclastic/carbonate basinal cycles: discussion with examples. *AAPG Bull.* 73, 1233–1246. doi:10.1306/44b4aa0f-170a-11d7-8645000102c1865d
- Dong, G., Chen, H., He, Y., Qing, Z., and Luo, J. (2007). Some problems on the study of the mixed siliciclastic carbonate sediments. *Adv. Earth Sci.* 22, 931. doi:10.11867/j.issn.1001-8166.2007.09.0931
- Du, X. F., Xu, C. G., Zhu, H. T., Xie, X. N., Zhu, X. M., Liu, K. Y., et al. (2020). Research advances of mixed siliciclastic and carbonate sediments in continental rift basins. *Earth Sci.* 45, 3509–3526. doi:10.3799/dqkx.2020.251
- Fang, S. Y. (2010). *Study on the technology of improving secondary oil recovery effect-taking Huatugou Oilfield in the west of Qaidam Basin as an Example*. Chengdu: Chengdu University of Technology. PhD dissertation.
- Feng, J. L., Cao, J., Hu, K., Chen, Y., Yang, S. Y., Liu, Y. T., et al. (2011a). Forming mechanism of middle-deep mixed rock reservoir in the Qaidam basin. *Acta Petrol. Sin.* 27, 2461–2472.
- Feng, J. L., Hu, K., Cao, J., Chen, Y., Wang, L. G., Zhang, Y., et al. (2011b). A review on mixed rocks of terrigenous clastics and carbonates and their petroleum-gas geological significance. *Geol. J. China Univ.* 17, 297. doi:10.16108/j.issn1006-7493.2011.02.016
- Feng, J. L., Cao, J., Hu, K., Peng, X. Q., Chen, Y., Wang, Y. F., et al. (2013). Dissolution and its impacts on reservoir formation in moderately to deeply buried strata of mixed siliciclastic-carbonate sediments, northwestern Qaidam Basin, northwest China. *Mar. Petroleum Geol.* 39, 124–137. doi:10.1016/j.marpetgeo.2012.09.002
- Fu, X., Du, X. F., Guan, D. Y., Wang, Q. M., and Ye, M. S. (2020). Depositional system, plane distribution and exploration significance of fan delta mixed siliciclastic-carbonate sediments in lacustrine basin: an example of Member 1-2 of Shahejie Formation in offshore Bohai Bay, Eastern China. *Earth Sci.* 45, 3706–3720. doi:10.3799/dqkx.2020.173
- Gao, G., Yang, S. R., and Qu, T. (2018). Research status of mixing sediments and their relationship with petroleum enrichment. *Geol. Sci. Technol. Inf.* 37, 82–88. doi:10.19509/j.cnki.dzqk.2018.0610
- Gierlowski-Kordesch, E., Finkelstein, D. B., Truchan Holland, J. J., and Kallini, K. D. (2014). Carbonate lake deposits associated with distal siliciclastic perennial-river systems. *J. Sediment. Res.* 83, 1114–1129. doi:10.2110/jsr.2013.81
- Karakaya, S., Ogiesoba, O. C., and Olariu, C. (2022). Lateral lithology heterogeneity due to autogenic processes in mixed carbonate and siliciclastic deposits of Cisco Group, the Eastern Shelf of the Permian Basin. *King Cty. north-central Texas[C]//SEG Int. Expo. Annu. Meet. SEG. D011S023R004*. doi:10.1190/image2022-3751846.1
- Karakaya, S., Ogiesoba, O. C., Olariu, C., and Bhattacharya, S. (2024). Generating 3D lithology probability volumes using poststack inversion, probabilistic neural networks, and Bayesian classification—a case study from the mixed carbonate and siliciclastic deposits of the Cisco Group of the Eastern Shelf of the Permian Basin, north-central Texas. *Geophysics* 89 (2), B131–B146. doi:10.1190/geo2023-0157.1
- Kjøll, H. J., Midtkandal, I., Planke, S., Millett, J., Mantou, B., and Anderskov, K. (2014). The interplay between siliciclastic and carbonate depositional systems: maastrichtian to Danian basin-floor sediments of the MID-Norwegian More Basin. *Basin Res.* 36, e12827. doi:10.1111/bre.12827
- Lebec, U., Lang, S. C., Paumard, V., O'Leary, M. J., Yokoyama, Y., Hacker, J., et al. (2023). Discovery of holocene ooid shoals in a siliciclastic delta, de grey river, north west shelf, Australia. *Geology* 51, 366–371. doi:10.1130/g50840.1

- Lee, Y. I., and Kim, J. C. (1992). Storm-influenced siliciclastic and carbonate ramp deposits, the lower ordovician dumugol formation, South Korea. *Sedimentology* 39, 951–969. doi:10.1111/j.1365-3091.1992.tb01990.x
- Li, Y., Gou, Y., Cao, Z., and Sun, X. (2009). Identification of algal limestone reservoir with logging in Yuexi area, Qaidam basin. *J. Southwest Petroleum Univ. Sci. and Technol. Ed.* 31, 56.
- Li, T., Huang, Z., Feng, Y., Chen, X., Ma, Q., Liu, B., et al. (2020). Reservoir characteristics and evaluation of fluid mobility in organic-rich mixed siliciclastic-carbonate sediments: a case study of the lacustrine Qiketai Formation in Shengbei Sag, Turpan-Hami Basin, Northwest China. *J. Petroleum Sci. Eng.* 185, 106667. doi:10.1016/j.petrol.2019.106667
- Li, Q. Q., Bao, Z. D., Xiao, Y. X., Chen, J. Y., Li, Z. C., Wang, Z. J., et al. (2021). Research advances and prospect of mixed deposition. *Acta Sedimentol. Sin.* 39, 153–167. doi:10.14027/j.issn.1000-0550.2020.140
- Li, Y., Huang, W., and Jiu, B. (2021). Factors that controlled deposition of lacustrine, mixed siliciclastic-carbonate sediments in the upper fourth member of the Eocene Shahejie Formation in the Zhanhua Sag, East China. *J. Paleolimnol.* 66, 55–70. doi:10.1007/s10933-021-00185-x
- Liu, Z. G., Zhang, Y. S., Song, G. Y., Li, S. M., Long, G. H., Zhao, J., et al. (2021). Mixed carbonate rocks lithofacies features and reservoirs controlling mechanisms in a saline lacustrine basin in Yingxi area, Qaidam Basin, NW China. *Petroleum Explor. Dev.* 48, 80–94. doi:10.1016/s1876-3804(21)60006-x
- Meng, Z., Feng, B., and Wang, G. (2009). Sedimentation of mixed bioclastic shallows of steep slope zone in Gubei Depression. *Petroleum Geol. Eng.* 23, 9–11.
- Mount, J. E. (1984). Mixing of siliciclastic and carbonate sediments in shallow shelf environments. *Geology* 12, 432–435. doi:10.1130/0091-7613(1984)12<432:mosacs>2.0.co;2
- Mount, J. (1985). Mixed siliciclastic and carbonate sediments: a proposed first-order textural and compositional classification. *Sedimentology* 32, 435–442. doi:10.1111/j.1365-3091.1985.tb00522.x
- Mutti, M., Vallati, M., Tomás, S., Galli, C., Bahniuk Rumbelsperger, A. M., Maerz, S., et al. (2023). Constraining depositional evolution and reservoir compartmentalization in a mixed carbonate-siliciclastic lacustrine system: the Yacoraite formation, Salta Group, NW Argentina. *Mar. Petroleum Geol.* 149, 106049. doi:10.1016/j.marpetgeo.2022.106049
- Palermo, D., Aigner, T., Geluk, M., Poeppelreiter, M., and Pipping, K. (2008). Reservoir potential of a lacustrine mixed carbonate/siliciclastic gas reservoir: the Lower Triassic Rogenstein in The Netherlands. *J. Petroleum Geol.* 31, 61–96. doi:10.1111/j.1747-5457.2008.00407.x
- Wang, Y. Q., Gong, Q. S., Xia, Z. Y., and Xiong, S. Y. (2012). Provenance analysis of oligocene sediments in western Qaidam Basin. *Geol. China* 39, 426–435.
- Wang, J., Zhang, D., Yang, S., Li, X., Shi, Y., Cui, J., et al. (2020). Sedimentary characteristics and genesis of the salt lake with the upper member of the Lower Ganhaigou Formation from Yingxi sag, Qaidam basin. *Mar. Petroleum Geol.* 111, 135–155. doi:10.1016/j.marpetgeo.2019.08.006
- Wang, Q. M., Du, X. F., and Wan, L. W. (2020). Characteristics of mixed sedimentary development and main control factors in lower third member of shahejie formation of southern slope belt of laizhouwan sag, Bohai sea. *Earth Sci.* 45, 3645–3662. doi:10.3799/dqkx.2020.187
- Wei, X., Li, Z., Ma, Y., Li, Y., Hu, J., Liu, K., et al. (2021). Sedimentology and sequence stratigraphy of the mixed clastic-carbonate deposits in the Late Paleozoic icehouse period: a case study from the northern Qaidam Basin. *China Geol.* 4, 1–13. doi:10.31035/cg2021068
- Wu, Y. Y., Lü, J. L., and Fang, X. (2019). Analysis of favorable facies belts in reservoir of lacustrine carbonate rocks-hybrid sediments: case study of Paleogene in Qaidam Basin. *Nat. Gas. Geosci.* 30, 1150–1157. doi:10.11764/j.issn.1672-1926.2019.05.019
- Wu, H., Liu, H., Wang, L., Gui, L., Yang, C., and Wang, L. (2022). Mixed carbonate-siliciclastic reservoir characterization and hydrocarbon accumulation process of the Ganhaigou area in the western Qaidam Basin, Tibet Plateau. *Carbonates Evaporites* 37, 26. doi:10.1007/s13146-022-00769-2
- Xu, W., Du, X. F., Huang, X. B., Song, Z., and Li, Z. (2019). Research Advances and Critical Issues of “mixed siliciclastic and carbonate sediments”. *Acta Sedimentol. Sin.* 37, 225–238. doi:10.14027/j.issn.1000-0550.2018.152
- Ye, M., Xie, X., Xu, C., Du, X., Du, X., and Song, Z. (2019). Sedimentary features and their controls in a mixed siliciclastic-carbonate system in a shallow lake area: an example from the BZ-X block in the Huanghekou Sag, Bohai Bay Basin, Eastern China. *Geol. J.* 54, 2016–2033. doi:10.1002/gj.3275
- Zhang, M., Yin, C. M., Shou, J. F., Chen, Z. L., and Zhang, Y. Z. (2004). Sedimentary facies of carbonate rocks of the paleogene and Neogene in western Qaidam Basin. *J. Palaeogeogr.* 6, 391–400.
- Zhao, F. (2015). Identification of Neogene mixed lacustrine carbonate in western Qaidam basin. *Carbonates Evaporites* 30, 281–285. doi:10.1007/s13146-014-0210-9